

ACCELERATED HIGH-INDEX SADDLE DYNAMICS METHOD FOR SEARCHING HIGH-INDEX SADDLE POINTS

YUE LUO*, LEI ZHANG†, AND XIANGCHENG ZHENG‡

Abstract. The High-index saddle dynamics (HiSD) method serves as an efficient tool for computing saddle points and constructing solution landscapes. Nevertheless, the conventional HiSD method often encounters slow convergence rates on ill-conditioned problems. To address this challenge, we propose an accelerated high-index saddle dynamics (A-HiSD) by incorporating the heavy ball method. We prove the linear stability theory of the continuous A-HiSD, and subsequently estimate the local convergence rate for the discrete A-HiSD. Our analysis demonstrates that the A-HiSD method exhibits a faster convergence rate compared to the conventional HiSD method, especially when dealing with ill-conditioned problems. We also perform various numerical experiments including the loss function of neural network to substantiate the effectiveness and acceleration of the A-HiSD method.

Key words. saddle point, saddle dynamics, heavy ball, acceleration, solution landscape

AMS subject classifications. 37M05, 37N30, 65L20

1. Introduction. Searching saddle points in various complex systems has attracted attentions in many scientific fields such as finding critical nuclei and transition pathways in phase transformations [10, 19, 43, 51, 63], protein folding [6, 47], Lennard-Jones clusters [7, 48], etc. In recent years, saddle points are also found to play an essential role in the field of deep learning for the analysis of loss landscape [12, 16, 67] and training strategies [11, 25, 26].

In general, there are two classes of approaches for finding saddle points: path-finding methods and surface walking methods. The former class is suitable for locating index-1 saddle points when initial and final states on the energy surface are available. It searches a discrete string connecting the initial and final points to find the minimum energy path. The representative methods include the string method [14] and the nudged elastic band method [23]. The latter class starts from a single point and utilizes first-order or second-order derivatives to search saddle points, such as the gentlest ascent method [15, 39], the eigenvector-following method [9], the minimax method [29], the activation-relaxation techniques [8], the iterative minimization formulation [17], and the dimer type method [18, 22, 61, 64].

Recently, the high-index saddle dynamics (HiSD) method [58] serves as a powerful tool for the calculation of high-index saddle points and the construction of solution landscape when combined with the downward and upward algorithms [56, 62]. It has been successfully extended for the saddle point calculations in non-gradient systems [57] and constrained systems [54, 66]. The HiSD method and solution landscape have been widely used in physical and engineering problems, including finding the defect configurations in liquid crystals [20, 21, 44, 50, 59], nucleation in quasicrystals [55], morphologies of confined diblock copolymers [52], excited states in rotating Bose-Einstein condensates [53].

It was demonstrated in [58] that a linearly stable steady state of the HiSD is an index- k saddle point. Furthermore, [32] proved that the local linear convergence rate

*Beijing International Center for Mathematical Research, Peking University, Beijing 100871, China (moonluo@pku.edu.cn)

†Beijing International Center for Mathematical Research, Center for Machine Learning Research, Center for Quantitative Biology, Peking University, Beijing 100871, China (zhangl@math.pku.edu.cn)

‡School of Mathematics, Shandong University, Jinan 250100, China (xzheng@sdu.edu.cn)

of the discrete HiSD method is $1 - \mathcal{O}(\frac{1}{\kappa})$, where $\kappa \geq 1$ is the ratio of absolute values of maximal and minimal eigenvalues of the Hessian at the saddle point, reflecting the curvature information around this saddle point. In practice, many examples show that HiSD method suffers from the slow convergence rate if the problem is ill-conditioned, that is, κ is large. Hence, it is meaningful to design reliable acceleration mechanisms for the HiSD method to treat ill-conditioned problems.

The heavy ball method (HB) is a simple but efficient acceleration strategy that is widely applied in the field of optimization. It integrates the information of previous search direction, i.e. the momentum term $\gamma(x^{(n)} - x^{(n-1)})$, in the current step of optimization. Polyak pointed out that invoking the HB method could improve the local linear convergence rate of the gradient descent method [37]. Till now, the HB method has become a prevalent acceleration strategy in various situations. For instance, many adaptive gradient methods in deep learning such as the Adam [27], AMSGrad [42] and AdaBound [31] adopt the idea of HB method. Nguyen et al. [35] proposed an accelerated residual method by combining the HB method with an extra gradient descent step and numerically verified the efficiency of this method.

In this paper, we propose an accelerated high-index saddle dynamics (A-HiSD) method based on the HB method to enhance the convergence rate of the conventional HiSD method, especially for ill-conditioned problems. At the continuous level, we prove that a linearly stable steady state of the A-HiSD is an index- k saddle point, showcasing the effectiveness of A-HiSD in searching saddle points. The key ingredient of our proof relies on technical eigenvalue analysis of the Jacobian operator of the dynamical system. Subsequently, we propose and analyze the discrete scheme of A-HiSD, indicating a faster local convergence rate in comparison with the original HiSD method. Novel induction hypothesis method and matrix analysis methods are applied to accommodate the locality of the assumptions in the problem. To substantiate the effectiveness and acceleration capabilities of A-HiSD, we conduct a series of numerical experiments, including benchmark examples and ill-conditioned problems such as the loss function of neural networks. These results provide mathematical and numerical analysis support for application of the A-HiSD in saddle point search for ill-conditioned problems.

The paper is organized as follows: in Section 2 we review the HiSD method briefly and present a detailed description of the A-HiSD method. Stability analysis of the A-HiSD dynamical system is discussed in Section 3. Local convergence rate estimates of the proposed algorithm are proved in Section 4. Several experiments are presented to substantiate the acceleration of the proposed method in Section 5. Conclusions and further discussions are given in Section 6.

2. Formulation of A-HiSD.

2.1. Review of HiSD. HiSD method provides a powerful instrument to search any-index saddle points. The HiSD for an index- k ($1 \leq k \in \mathbb{N}$) saddle point of the energy function $E(x)$ reads [58]

$$(2.1) \quad \begin{cases} \dot{x} = -\beta \left(I - 2 \sum_{i=1}^k v_i v_i^\top \right) \nabla E(x), \\ \dot{v}_i = -\zeta \left(I - v_i v_i^\top - 2 \sum_{j=1}^{i-1} v_j v_j^\top \right) \nabla^2 E(x) v_i, \quad 1 \leq i \leq k, \end{cases}$$

where β and ζ are positive relaxation parameters. The continuous formulation (2.1) is discussed in details in [58], and the convergence rate and error estimates of the discrete algorithm are analyzed in [32, 65].

Algorithm 2.1 HiSD for an index- k saddle point

Input: $k \in \mathbb{N}$, $x^{(0)} \in \mathbb{R}^d$, $\{\hat{v}_i^{(0)}\}_{i=1}^k \subset \mathbb{R}^d$ satisfying $\hat{v}_i^{(0)\top} \hat{v}_j^{(0)} = \delta_{ij}$.

for $n = 0, 1, \dots, T-1$ **do**

$$x^{(n+1)} = x^{(n)} - \beta \left(I - 2 \sum_{i=1}^k \hat{v}_i^{(n)} \hat{v}_i^{(n)\top} \right) \nabla E(x^{(n)});$$

$$\{\hat{v}_i^{(n+1)}\}_{i=1}^k = \text{EigenSol}(\{\hat{v}_i^{(n)}\}_{i=1}^k, \nabla^2 E(x^{(n+1)})).$$

Return: $x^{(T)}$

The discrete scheme of HiSD method is shown in Algorithm 2.1. “EigenSol” represents some eigenvector solver with initial values $\{\hat{v}_i^{(n)}\}_{i=1}^k$ to compute eigenvectors corresponding to the first k smallest eigenvalues of $\nabla^2 E(x^{(n+1)})$, such as the simultaneous Rayleigh-quotient iterative minimization method (SIRQIT) [30] and locally optimal block preconditioned conjugate gradient (LOBPCG) method [28].

2.2. Algorithm of A-HiSD. Inspired by the simple implementation and the efficient acceleration phenomenon of the HB method, we propose the A-HiSD method described in Algorithm 2.2.

Algorithm 2.2 A-HiSD for an index- k saddle point

Input: $k \in \mathbb{N}$, $x^{(0)} \in \mathbb{R}^d$, orthonormal vectors $\{v_i^{(0)}\}_{i=1}^k \subset \mathbb{R}^d$.

1: Set $x^{(-1)} = x^{(0)}$.

2: **for** $n = 0, 1, \dots, T-1$ **do**

$$3: \quad x^{(n+1)} = x^{(n)} - \beta \left(I - 2 \sum_{i=1}^k v_i^{(n)} v_i^{(n)\top} \right) \nabla E(x^{(n)}) + \gamma(x^{(n)} - x^{(n-1)});$$

$$4: \quad \{v_i^{(n+1)}\}_{i=1}^k = \text{EigenSol}(\{v_i^{(n)}\}_{i=1}^k, \nabla^2 E(x^{(n+1)})).$$

Return: $x^{(T)}$

From the perspective of algorithm implementation, the only difference between A-HiSD method and HiSD method is the update formula of the position variable $x^{(n)}$. The A-HiSD method integrates the information of previous search direction in the current step, i.e. the momentum term $\gamma(x^{(n)} - x^{(n-1)})$, motivated by the HB method. Due to this modification, a significant acceleration is expected with the proper choice of the step size parameter β and momentum parameter γ . We will perform numerical analysis and numerical experiments in the following sections.

From the continuous level, the HB method is highly connected with a first-order ordinary differential equation system due to the presence of multiple steps [33]. Following this idea, we introduce the continuous A-HiSD system for an index- k saddle point:

$$(2.2) \quad \begin{cases} \dot{x} = m, \\ \dot{m} = -\alpha_1 m - \alpha_2 \left(I - 2 \sum_{i=1}^k v_i v_i^\top \right) \nabla E(x), \\ \dot{v}_i = -\zeta \left(I - v_i v_i^\top - 2 \sum_{j=1}^{i-1} v_j v_j^\top \right) H(x, v_i, l), \quad i = 1, 2, \dots, k, \\ \dot{l} = -l, \end{cases}$$

where $H(x, v, l)$ is the dimer approximation for the Hessian-vector product $\nabla^2 E(x)v$ [22, 58]

$$(2.3) \quad \nabla^2 E(x)v \approx H(x, v, l) = \frac{1}{2l} [\nabla E(x + lv) - \nabla E(x - lv)].$$

Here α_1 , α_2 and ζ are positive relaxation parameters.

REMARK 1. *To see the relations between the continuous and discrete formulations of the position variable in (2.2) and the Algorithm 2.2, respectively, we first combine the first two equations in (2.2) to obtain*

$$\ddot{x} = -\alpha_1 \dot{x} - \alpha_2 \left(I - 2 \sum_{i=1}^k v_i v_i^\top \right) \nabla E(x).$$

Then we discretize this equation with the step size Δt to obtain

$$\frac{x^{(n+1)} - 2x^{(n)} + x^{(n-1)}}{(\Delta t)^2} = -\alpha_1 \frac{x^{(n)} - x^{(n-1)}}{\Delta t} - \alpha_2 \left(I - 2 \sum_{i=1}^k v_i v_i^\top \right) \nabla E(x).$$

If we set $\beta = \alpha_2(\Delta t)^2$ and $\gamma = 1 - \alpha_1 \Delta t$, the scheme of the position variable in Algorithm 2.2 is consistent with the above scheme. Therefore, the formulation of the position variable in (2.2) is indeed the continuous version (or the limit case when $\Delta t \rightarrow 0^+$) of the A-HiSD algorithm.

3. Linear stability analysis of A-HiSD. We prove that the linearly stable steady state of (2.2) is exactly an index- k saddle point of E , which substantiates the effectiveness of (2.2) (and thus its discrete version in Algorithm 2.2) in finding high-index saddle points.

THEOREM 3.1. *Assume that $E(x)$ is a C^3 function, $\{v_i^*\}_{i=1}^k \subset \mathbb{R}^d$ satisfy $\|v_i^*\|_2 = 1$ for $1 \leq i \leq k$, where $\|\cdot\|_2$ denotes the vector Euclidean norm. The Hessian $\nabla^2 E(x^*)$ is non-degenerate with the eigenvalues $\lambda_1^* < \dots < \lambda_k^* < 0 < \lambda_{k+1}^* \leq \dots \leq \lambda_d^*$, and $\alpha_1, \alpha_2, \zeta > 0$ satisfy $\alpha_1^2 \leq 4\alpha_2\mu$ where $\mu^* = \min\{|\lambda_i^*|, i = 1, \dots, k\}$. Then the following two statements are equivalent:*

- (A) $(x^*, m^*, v_1^*, \dots, v_k^*, l^*)$ is a linearly stable steady state of the A-HiSD (2.2);
- (B) x^* is an index- k saddle point of E , $\{v_i^*\}_{i=1}^k$ are eigenvectors of $\nabla^2 E(x^*)$ with the corresponding eigenvalues $\{\lambda_i^*\}_{i=1}^k$ and $m^* = l^* = 0$.

Proof. To determine the linear stability of A-HiSD (2.2), we calculate its Jacobian

operator as follows

$$(3.1) \quad J = \frac{\partial(\dot{x}, \dot{m}, \dot{v}_1, \dot{v}_2, \dots, \dot{v}_k, \dot{l})}{\partial(x, m, v_1, v_2, \dots, v_k, l)} = \begin{bmatrix} 0 & I & 0 & 0 & \dots & 0 & 0 \\ J_{mx} & -\alpha_1 I & J_{m1} & J_{m2} & \dots & J_{mk} & 0 \\ J_{1x} & 0 & J_{11} & 0 & \dots & 0 & J_{1l} \\ J_{2x} & 0 & J_{21} & J_{22} & \dots & 0 & J_{2l} \\ \vdots & \vdots & \vdots & \vdots & \vdots & \vdots & \vdots \\ J_{kx} & J_{km} & J_{k1} & J_{k2} & \dots & J_{kk} & J_{kl} \\ 0 & 0 & 0 & 0 & 0 & 0 & -1 \end{bmatrix},$$

where part of the blocks are presented in details as follows

$$\begin{aligned} J_{mx} &= \partial_x \dot{m} = -\alpha_2 \mathcal{P}_k \nabla^2 E(x), \\ J_{mi} &= \partial_{v_i} \dot{m} = 2\alpha_2 (v_i^\top \nabla E(x) I + v_i \nabla E(x)^\top), \\ J_{ii} &= \partial_{v_i} \dot{v}_i = -\zeta(\mathcal{P}_{i-1} - v_i v_i^\top) \partial_{v_i} H(x, v_i, l) + \zeta(v_i^\top H(x, v_i, l) I + v_i H(x, v_i, l)^\top), \\ J_{il} &= -\zeta(\mathcal{P}_{i-1} - v_i v_i^\top) \partial_l H(x, v_i, l). \end{aligned}$$

Here we use the notation $\mathcal{P}_s := I - 2 \sum_{j=1}^s v_j v_j^\top$ for $1 \leq s \leq k$ and $\mathcal{P}_0 = I$. Derivatives of $H(x, v_i, l)$ with respect to different variables are

$$\begin{aligned} \partial_l H(x, v_i, l) &= \frac{\nabla^2 E(x + lv_i) + \nabla^2 E(x - lv_i)}{2l} v_i - \frac{\nabla E(x + lv_i) - \nabla E(x - lv_i)}{2l^2}, \\ \partial_{v_i} H(x, v_i, l) &= \frac{\nabla^2 E(x + lv_i) + \nabla^2 E(x - lv_i)}{2}. \end{aligned}$$

By the smoothness of the energy function $E(x)$ and Taylor expansions, we could directly verify the following limits for future use

$$(3.2) \quad \lim_{l \rightarrow 0^+} H(x, v_i, l) = \nabla^2 E(x) v_i, \quad \lim_{l \rightarrow 0^+} \partial_l H(x, v_i, l) = 0, \quad \lim_{l \rightarrow 0^+} \partial_{v_i} H(x, v_i, l) = \nabla^2 E(x).$$

We firstly derive (A) from (B). Under the conditions of (B), we have $\nabla E(x^*) = 0$, $\nabla^2 E(x^*) v_i^* = \lambda_i^* v_i^*$ for $1 \leq i \leq k$ and $m^* = l^* = 0$ such that $(x^*, m^*, v_1^*, v_2^*, \dots, v_k^*, l^*)$ is a steady state of (2.2). To show the linear stability, we remain to show that all eigenvalues of J^* , the Jacobian (3.1) at this steady state, have negative real parts. From $\nabla E(x^*) = 0$ and $l = 0$, we observe that J_{mi}^* and J_{il}^* are zero matrices such that J^* is in the form of

$$(3.3) \quad J^* = \begin{bmatrix} Z_1^* & 0 \\ G^* & Z_2^* \end{bmatrix} \text{ with } Z_1^* := \begin{bmatrix} 0 & I \\ J_{mx}^* & -\alpha_1 I \end{bmatrix} \text{ and } Z_2^* := \begin{bmatrix} J_{11}^* & 0 & \dots & 0 & 0 \\ J_{21}^* & 0 & \dots & 0 & 0 \\ \vdots & \vdots & \vdots & \vdots & \vdots \\ J_{k1}^* & J_{k2}^* & \dots & J_{kk}^* & 0 \\ 0 & 0 & 0 & 0 & -1 \end{bmatrix}.$$

Therefore the spectrum of J^* is completely determined by Z_1^* and Z_2^* . By (3.2) and the spectrum decomposition theorem $\nabla^2 E(x^*) = \sum_{i=1}^d \lambda_i^* v_i^* v_i^{*\top}$, the diagonal block J_{ii}^* of Z_2^* could be expanded as

$$J_{ii}^* = -\zeta(\mathcal{P}_{i-1}^* - v_i^* v_i^{*\top}) \nabla^2 E(x^*) + \zeta(v_i^{*\top} \nabla^2 E(x^*) v_i^* I + v_i^* (\nabla^2 E(x^*) v_i^*)^\top)$$

$$= -\zeta\left(\nabla^2 E(x^*) - 2 \sum_{j=1}^i \lambda_j^* v_j^* v_j^{*\top} - \lambda_i^* I\right),$$

which means J_{ii}^* is equipped with the following eigenvalues

$$(3.4) \quad \{\zeta(\lambda_1^* + \lambda_i^*), \dots, \zeta(\lambda_i^* + \lambda_i^*), \zeta(\lambda_i^* - \lambda_{i+1}^*), \dots, \zeta(\lambda_i^* - \lambda_d^*)\}, \quad 1 \leq i \leq k.$$

By the assumptions of this theorem, all these eigenvalues are negative such that all eigenvalues of Z_2^* are negative. Then we apply the expansion of J_{mx}^*

$$(3.5) \quad J_{mx}^* = -\alpha_2 \left(-\sum_{i=1}^k \lambda_i^* v_i^* v_i^{*\top} + \sum_{j=k+1}^d \lambda_j^* v_j^* v_j^{*\top} \right)$$

to partly diagonalize Z_1^* as

$$(3.6) \quad \begin{bmatrix} V^* & 0 \\ 0 & V^* \end{bmatrix}^\top Z_1^* \begin{bmatrix} V^* & 0 \\ 0 & V^* \end{bmatrix} = \begin{bmatrix} 0 & I \\ D^* & -\alpha_1 I \end{bmatrix} =: \tilde{Z}_1^*,$$

where $V^* = [v_1^*, \dots, v_d^*]$ is the orthogonal matrix, $D^* := \text{diag}\{d_i^*\}_{i=1}^d$ is the diagonal matrix with the entries $\{\alpha_2 \lambda_1^*, \dots, \alpha_2 \lambda_k^*, -\alpha_2 \lambda_{k+1}^*, \dots, -\alpha_2 \lambda_d^*\}$ and, after a series of permutations, \tilde{Z}_1^* is similar to a block diagonal matrix with d blocks defined by

$$(3.7) \quad D_i^* = \begin{bmatrix} 0 & 1 \\ d_i^* & -\alpha_1 \end{bmatrix}, \quad 1 \leq i \leq d.$$

The eigenvalues of D_i^* are roots of $x^2 + \alpha_1 x - d_i^* = 0$. Since $d_i^* \leq -\alpha_2 \mu^* < 0$ for $1 \leq i \leq d$, we have $\Delta_i = \alpha_1^2 + 4d_i^* \leq \alpha_1^2 - 4\alpha_2 \mu^* \leq 0$, which implies that the roots of D_i^* are either two same real numbers or conjugate complex numbers. In both cases, the real parts of the roots are negative due to $\alpha_1 > 0$, which in turn implies that all eigenvalues of \tilde{Z}_1^* have negative real parts. In conclusion, the real parts of all eigenvalues of J^* are negative, which indicates that $(x^*, m^*, v_1^*, v_2^*, \dots, v_k^*, l^*)$ is a linearly stable steady state of (2.2) and thud proves (A).

To prove (B) from (A), we suppose that $(x^*, m^*, v_1^*, v_2^*, \dots, v_k^*, l^*)$ is a linearly stable steady state of (2.2), which leads to $m^* = l^* = 0$ and

$$(3.8) \quad (\mathcal{P}_{i-1}^* - v_i^* v_i^{*\top}) \nabla^2 E(x^*) v_i^* = 0$$

for $1 \leq i \leq k$. We intend to apply the mathematical induction to prove

$$(3.9) \quad \nabla^2 E(x^*) v_i^* = z_i^* v_i^*, \quad z_i = v_i^{*\top} \nabla^2 E(x^*) v_i^* \neq 0, \quad v_i^{*\top} v_j^* = 0, \quad 1 \leq j < i \leq k,$$

i.e. $\{(z_i^*, v_i^*)\}_{i=1}^k$ are eigen pairs of $\nabla^2 E(x^*)$. For (3.8) with $i = 1$, we have $\nabla^2 E(x^*) v_1^* = z_1^* v_1^*$ with $z_1^* = v_1^{*\top} \nabla^2 E(x^*) v_1^*$ being an eigenvalue of $\nabla^2 E(x^*)$. Since $\nabla^2 E(x^*)$ is non-degenerate, $z_1^* \neq 0$. (3.9) holds true at $i = 1$. Assume that (3.9) holds for $i = 1, 2, \dots, m-1$. Then (3.8) with $i = m$ yields

$$(3.10) \quad \mathcal{P}_{m-1}^* \nabla^2 E(x^*) v_m^* = \left(\nabla^2 E(x^*) - 2 \sum_{j=1}^{m-1} z_j^* v_j^* v_j^{*\top} \right) v_m^* = z_m^* v_m^*,$$

where $z_m^* = v_m^{*\top} \nabla^2 E(x^*) v_m^*$, which implies v_m^* is the eigenvector of $\mathcal{P}_{m-1}^* \nabla^2 E(x^*)$. However, since $\{v_j^*\}_{j=1}^{m-1}$ are eigenvectors of $\nabla^2 E(x^*)$, $\nabla^2 E(x^*)$ and $\mathcal{P}_{m-1}^* \nabla^2 E(x^*)$

share the same eigenvectors such that v_m^* is also an eigenvector of $\nabla^2 E(x^*)$ and there exists an eigenvalue μ_m^* such that $\nabla^2 E(x^*)v_m^* = \mu_m^* v_m^*$. we multiply $v_m^{*\top}$ on both sides of this equation and utilize $\|v_m^*\|_2 = 1$ to obtain $v_m^{*\top} \nabla^2 E(x^*)v_m^* = \mu_m^* \|v_m^*\|_2^2 = \mu_m^*$, that is, $z_m^* = \mu_m^*$. Combining (3.10) and $\nabla^2 E(x^*)v_m^* = z_m^* v_m^*$, we have $\sum_{j=1}^{m-1} z_j^* (v_j^{*\top} v_m^*) v_j^* = 0$, and we multiply $(v_s^*)^\top$ for $1 \leq s \leq m-1$ on both sides of this equation and apply (3.9) to get $v_s^{*\top} v_m^* = 0$ for $1 \leq s \leq m-1$. Therefore, (3.9) holds for $i = m$ and thus for any $1 \leq i \leq k$.

As a result of (3.9), \mathcal{P}_k is an orthogonal matrix, which, together with the right-hand side of the dynamics of m in (2.2) with $m^* = 0$, indicates $\nabla E(x^*) = 0$, i.e. x^* is a critical point of E .

It remains to check that x^* is an index- k saddle point of E . From $l^* = 0$ and $\nabla E(x^*) = 0$, J^* could be divided as (3.3) and the linear stability condition in (A) implies that all eigenvalues of Z_1^* and Z_2^* have negative real parts. Since (3.9) indicates that $\{(z_i^*, v_i^*)\}_{i=1}^k$ are eigen-pairs of $\nabla^2 E(x^*)$, we denote $z_{k+1}^* \leq \dots \leq z_d^*$ as the remaining eigenvalues of $\nabla^2 E(x^*)$. By the derivation of (3.5), eigenvalues of J_{mx}^* are $\{\alpha_2 z_1^*, \dots, \alpha_2 z_k^*, -\alpha_2 z_{k+1}^*, \dots, -\alpha_2 z_d^*\}$. Following the discussions among (3.6)–(3.7), eigenvalues of Z_1^* are roots of $x^2 + \alpha_1 x - d_i^* = 0$ for $1 \leq i \leq d$ with $d_i^* = \alpha_2 z_i^*$ for $i \leq k$ and $d_i^* = -\alpha_2 z_i^*$ for $k < i \leq d$. To ensure that all eigenvalues have negative real parts, d_i must be negative, which implies $z_i^* < 0$ for $i \leq k$ and $z_i^* > 0$ for $k < i \leq d$, that is, x^* is an index- k saddle point.

Finally, it follows from (3.4) that $\{\zeta(z_i^* + z_1^*), \dots, \zeta(z_i^* + z_k^*), \zeta(z_i^* - z_{k+1}^*), \dots, \zeta(z_i^* - z_d^*)\}$ are eigenvalues of J_{ii}^* for $1 \leq i \leq k$. To ensure that all eigenvalues are negative, we have $z_1^* < z_2^* < \dots < z_k^*$ such that z_i^* match λ_i^* , i.e., $z_i^* = \lambda_i^*$ for $1 \leq i \leq k$, which proves (B) and thus completes the proof. \square

4. Local convergence analysis of discrete A-HiSD. In this section, we present numerical analysis of the discrete Algorithm 2.2. Results on some mild conditions indicates that our proposed method has a faster local convergence rate compared with the vanilla HiSD method. We introduce the following assumptions for numerical analysis, which are standard to analyze the convergence behavior of iterative algorithms [32, 33].

ASSUMPTION 1. *The initial position $x^{(0)}$ locates in a neighborhood of the index- k saddle point x^* , i.e., $x^{(0)} \in U(x^*, \delta) = \{x \mid \|x - x^*\|_2 < \delta\}$ for some $\delta > 0$ such that*

- (i) *There exists a constant $M > 0$ such that $\|\nabla^2 E(x) - \nabla^2 E(y)\|_2 \leq M \|x - y\|_2$ for all $x, y \in U(x^*, \delta)$, where $\|\cdot\|_2$ denotes the Euclidean norm for vectors and the operator norm for matrices;*
- (ii) *For any $x \in U(x^*, \delta)$, eigenvalues $\{\lambda_i\}_{i=1}^d$ of $\nabla^2 E(x)$ satisfy $\lambda_1 \leq \dots \leq \lambda_k < 0 < \lambda_{k+1} \leq \dots \leq \lambda_d$ and there exist positive constants $0 < \mu < L$ such that $|\lambda_i| \in [\mu, L]$ for $1 \leq i \leq d$.*

Assumption 1 leads to an essential corollary on the Lipschitz continuity of the orthogonal projection on eigen subspace, which is stated in Corollary 4.2. The core of its proof is the Davis-Kahan theorem [46], which captures the sensitivity of eigenvectors under matrix perturbations. Here we adopt an variant of the Davis-Kahan theorem stated as following.

THEOREM 4.1. [60, Theorem 2] *Let $\Sigma, \hat{\Sigma} \in \mathbb{R}^{d \times d}$ be symmetric, with eigenvalues $\lambda_d \geq \dots \geq \lambda_1$ and $\hat{\lambda}_d \geq \dots \geq \hat{\lambda}_1$ respectively. Fix $1 \leq r \leq s \leq d$ and assume that $\min(\lambda_r - \lambda_{r-1}, \lambda_{s+1} - \lambda_s) > 0$, where we define $\lambda_0 = -\infty$ and $\lambda_{d+1} = +\infty$. Let $p = s - r + 1$, and let $V = [v_r, v_{r+1}, \dots, v_s] \in \mathbb{R}^{d \times p}$ and $\hat{V} = [\hat{v}_r, \hat{v}_{r+1}, \dots, \hat{v}_s] \in \mathbb{R}^{d \times p}$ have orthonormal columns satisfying $\Sigma v_j = \lambda_j v_j$ and $\hat{\Sigma} \hat{v}_j = \hat{\lambda}_j \hat{v}_j$ for $j = r, r+1, \dots, s$.*

Then

$$\|VV^\top - \hat{V}\hat{V}^\top\|_F \leq \frac{2\sqrt{2}\min(p^{1/2}\|\hat{\Sigma} - \Sigma\|_2, \|\hat{\Sigma} - \Sigma\|_F)}{\min(\lambda_r - \lambda_{r-1}, \lambda_{s+1} - \lambda_s)},$$

where $\|\cdot\|_F$ is the matrix Frobenius norm, i.e. $\|A\|_F = \sqrt{\text{tr}(AA^\top)}$.

COROLLARY 4.2. Fix any $x, y \in U(x^*, \delta)$ in Assumption 1. Denote the orthogonal projections $\mathcal{N}(x) = \sum_{i=1}^k u_{x,i} u_{x,i}^\top$ and $\mathcal{N}(y) = \sum_{i=1}^k u_{y,i} u_{y,i}^\top$ where $\{u_{x,i}\}_{i=1}^k$ and $\{u_{y,i}\}_{i=1}^k$ are two sets of orthonormal eigenvectors corresponding to the first k smallest eigenvalues of $\nabla^2 E(x)$ and $\nabla^2 E(y)$, respectively, i.e., $\nabla^2 E(x)u_{x,i} = \lambda_{x,i}u_{x,i}$, $\nabla^2 E(y)u_{y,i} = \lambda_{y,i}u_{y,i}$, $i = 1, \dots, k$, $\{\lambda_{x,i}\}_{i=1}^k$ and $\{\lambda_{y,i}\}_{i=1}^k$ are corresponding eigenvalues. Then

$$\|\mathcal{N}(x) - \mathcal{N}(y)\|_2 \leq \frac{\sqrt{2k}M}{\mu} \|x - y\|_2.$$

Proof. We apply Theorem 4.1 by setting $\Sigma = \nabla^2 E(x)$, $V = [u_{x,1}, \dots, u_{x,k}]$ and $\hat{\Sigma} = \nabla^2 E(y)$, $\hat{V} = [u_{y,1}, \dots, u_{y,k}]$. Then $VV^\top = \mathcal{N}(x)$ and $\hat{V}\hat{V}^\top = \mathcal{N}(y)$. By (ii) of Assumption 1, $\lambda_{x,k} \leq -\mu < \mu \leq \lambda_{x,k+1}$. Hence $\min(\lambda_{x,k+1} - \lambda_{x,k}, \lambda_{x,1} - \lambda_{x,0}) \geq 2\mu$. We have

$$\|\mathcal{N}(x) - \mathcal{N}(y)\|_2 \leq \|\mathcal{N}(x) - \mathcal{N}(y)\|_F \leq \frac{2\sqrt{2k}}{2\mu} \|\nabla^2 E(x) - \nabla^2 E(y)\|_2$$

where the first inequality follows because the matrix 2-norm is less than Frobenius norm, and the second from the application of Theorem 4.1. We end our proof by (ii) of Assumption 1. \square

We refer the following useful lemma to support our analysis.

LEMMA 4.3. [49, Theorem 5] Let $A := \begin{bmatrix} (1+\gamma)I - \beta G & -\gamma I \\ I & 0 \end{bmatrix} \in \mathbb{R}^{2d \times 2d}$ where $G \in \mathbb{R}^{d \times d}$ is a positive semidefinite matrix. If $\beta \in (0, 2/\lambda_{\max}(G))$, then the operator norm of A^k could be bounded as $\|A^k\|_2 \leq D_0(\sqrt{\gamma})^k$ for $1 \geq \gamma > \max\{(1 - \sqrt{\beta\lambda_{\max}(G)})^2, (1 - \sqrt{\beta\lambda_{\min}(G)})^2\}$ where

$$D_0 := \frac{2(1+\gamma)}{\sqrt{\min\{h(\gamma, \beta\lambda_{\min}(G)), h(\gamma, \beta\lambda_{\max}(G))\}}} \geq 1,$$

$\lambda_{\max}(G)$ and $\lambda_{\min}(G)$ are the largest and the smallest eigenvalues of G , respectively, and the function $h(\beta, z)$ is defined as $h(\gamma, z) := -(\gamma - (1 - \sqrt{z})^2)(\gamma - (1 + \sqrt{z})^2)$.

Based on Lemma 4.3, we derive a generalized result using the bounds of eigenvalues rather than their exact values.

COROLLARY 4.4. Assume that the eigenvalues of G in Lemma 4.3 satisfy $0 < \mu \leq \lambda_{\min}(G) \leq \lambda_{\max}(G) \leq L$. Then $\|A^k\|_2 \leq C_0(\sqrt{\gamma})^k$ for $1 \geq \gamma > \max\{(1 - \sqrt{\beta L})^2, (1 - \sqrt{\beta\mu})^2\}$ if $\beta \in (0, 2/L)$, where A and h are defined in Lemma 4.3 and

$$C_0 := \frac{2(1+\gamma)}{\sqrt{\min\{h(\gamma, \beta\mu), h(\gamma, \beta L)\}}} \geq 1.$$

In particular, choosing

$$(4.1) \quad \sqrt{\beta} = \frac{2}{\sqrt{L} + \sqrt{\mu}}, \quad \sqrt{\gamma} = 1 - \frac{2}{\sqrt{\kappa} + 1} + \varepsilon$$

with $\varepsilon \in (0, \frac{1}{\sqrt{\kappa}+1})$ and $\kappa := L/\mu \geq 1$ leads to

$$(4.2) \quad C_0 \leq \frac{2\sqrt{2}(\sqrt{\kappa}+1)^{1/2}}{\sqrt{3}\varepsilon} =: K.$$

Proof. Since h is a concave quadratic function with respect to z and $h(\gamma, z) > 0$ if γ is chosen under the assumptions and $z \in [\beta\mu, \beta L]$, the minimum of $h(\gamma, \cdot)$ on an interval must occur at end points of this interval. Consequently, $0 < \mu \leq \lambda_{\min}(G) \leq \lambda_{\max}(G) \leq L$ leads to $1 \leq D_0 \leq C_0$ where D_0 is given in Lemma 4.3. Furthermore, since $|1 - \sqrt{\beta}q|$ is a convex function with respect to q , we have

$$\max\{|1 - \sqrt{\beta\lambda_{\min}(G)}|, |1 - \sqrt{\beta\lambda_{\max}(G)}|\} \leq \max\{|1 - \sqrt{\beta\mu}|, |1 - \sqrt{\beta L}|\},$$

which proves the first statement of this corollary.

We then calculate $h(\gamma, \beta\mu)$ and $h(\gamma, \beta L)$ under the particular choice (4.1) of the parameters, which satisfy the constraints of this corollary by direct calculations. Since

$$\begin{aligned} \gamma - (1 - \sqrt{\beta\mu})^2 &= (1 - \frac{2}{\sqrt{\kappa}+1} + \varepsilon)^2 - (1 - \frac{2}{\sqrt{\kappa}+1})^2 = \varepsilon(2 - \frac{4}{\sqrt{\kappa}+1} + \varepsilon) \geq \varepsilon^2, \\ (1 + \sqrt{\beta\mu})^2 - \gamma &= (1 + \frac{2}{\sqrt{\kappa}+1})^2 - (1 - \frac{2}{\sqrt{\kappa}+1} + \varepsilon)^2 \\ &= (\frac{4}{\sqrt{\kappa}+1} - \varepsilon)(2 + \varepsilon) \geq \frac{3(2 + \varepsilon)}{\sqrt{\kappa}+1}, \end{aligned}$$

where we used $\frac{4}{\sqrt{\kappa}+1} \leq 2$ and $\varepsilon < \frac{1}{\sqrt{\kappa}+1}$, we have $h(\gamma, \beta\mu) \geq \varepsilon^2(2 + \varepsilon)\frac{3}{\sqrt{\kappa}+1}$. Similarly,

$$\begin{aligned} \gamma - (1 - \sqrt{\beta L})^2 &= \varepsilon(2 - \frac{4}{\sqrt{\kappa}+1} + \varepsilon) \geq \varepsilon^2, \\ (1 + \sqrt{\beta L})^2 - \gamma &= (2 - \varepsilon)(2 + \varepsilon + \frac{2\sqrt{\kappa}-2}{\sqrt{\kappa}+1}) \geq (2 - \varepsilon)(2 + \varepsilon) \geq \frac{3(2 + \varepsilon)}{\sqrt{\kappa}+1}, \end{aligned}$$

which lead to $h(\gamma, \beta L) \geq \varepsilon^2(2 + \varepsilon)\frac{3}{\sqrt{\kappa}+1}$. Consequently, C_0 could be further bounded as

$$C_0 = \frac{2(1 + \gamma)}{\sqrt{\min\{h(\gamma, \beta\mu), h(\gamma, \beta L)\}}} \leq \frac{2(1 + \gamma)(\sqrt{\kappa}+1)^{1/2}}{\sqrt{3\varepsilon^2(\varepsilon + 2)}} \leq \frac{2\sqrt{2}(\sqrt{\kappa}+1)^{1/2}}{\sqrt{3}\varepsilon},$$

which completes the proof. \square

We now turn to state our main results. We first reformulate the recurrence relation of the proposed algorithm in Theorem 4.5, based on which we prove the convergence rate of the proposed method in Theorem 4.6. We make the following assumption on Algorithm 2.2 in the analysis:

ASSUMPTION 2. $\{v_i^{(n)}\}_{i=1}^k$ are exact values of the first k smallest eigenvectors of $\nabla^2 E(x^{(n)})$ in each iteration in Algorithm 2.2, i.e. the error in “EigenSol” in Algorithm 2.2 is neglected.

The Assumption 2 helps to simplify the numerical analysis and highlight the ideas and techniques in the derivation of convergence rates. In practice, approximate eigenvectors computed from the “EigenSol” in Algorithm 2.2 should be considered but leads to more technical calculations in analyzing the convergence rates, see e.g. [32]. This extension will be investigated in the future work.

THEOREM 4.5. *The dynamics of x in Algorithm 2.2 could be written as*

$$(4.3) \quad \begin{bmatrix} x^{(n+1)} - x^* \\ x^{(n)} - x^* \end{bmatrix} = \begin{bmatrix} (1+\gamma)I - \beta A_* & -\gamma I \\ I & 0 \end{bmatrix} \begin{bmatrix} x^{(n)} - x^* \\ x^{(n-1)} - x^* \end{bmatrix} + \begin{bmatrix} p^{(n)} \\ 0 \end{bmatrix}$$

where $A_* = \mathcal{P}^* \nabla^2 E(x^*)$, $p_n = \beta(A_* - \tilde{A}_n)(x^{(n)} - x^*)$ and $\tilde{A}_n = \mathcal{P}_n \int_0^1 \nabla^2 E(x^* + (x^{(n)} - x^*)t) dt$ with

$$\mathcal{P}_n := I - 2 \sum_{i=1}^k v_i^{(n)} v_i^{(n)\top}, \quad \mathcal{P}^* := I - 2 \sum_{i=1}^k v_i^* v_i^{*\top},$$

where $\{v_i^*\}_{i=1}^k$ are the first k smallest eigenvectors of $\nabla^2 E(x^*)$.

Furthermore, if $x^{(n)} \in U(x^*, \delta)$ mentioned in ASSUMPTION 1 and the Assumption 2 holds, we have

$$(4.4) \quad \|p^{(n)}\|_2 \leq \beta C_1 \|x^{(n)} - x^*\|_2^2, \quad C_1 := \left(\frac{2\sqrt{2k}L}{\mu} + \frac{1}{2} \right) M.$$

Proof. By the integral residue of the Taylor expansion, we obtain

$$\nabla E(x^{(n)}) - \nabla E(x^*) = \left[\int_0^1 \nabla^2 E(x^* + t(x^{(n)} - x^*)) dt \right] (x^{(n)} - x^*).$$

As x^* is a critical point, we apply $\nabla E(x^*) = 0$ to reformulate the dynamics of x in Algorithm 2.2 as

$$(4.5) \quad \begin{aligned} x^{(n+1)} - x^* &= x^{(n)} - x^* - \beta \mathcal{P}_n \nabla E(x^{(n)}) + \gamma(x^{(n)} - x^{(n-1)}) \\ &= (I - \beta \tilde{A}_n) (x^{(n)} - x^*) + \gamma(x^{(n)} - x^{(n-1)}) \\ &= [(1+\gamma)I - \beta \tilde{A}_n] (x^{(n)} - x^*) - \gamma(x^{(n-1)} - x^*) \end{aligned}$$

where \tilde{A}_n is given in this theorem. We then transform (4.5) into the matrix form to obtain a single step formula

$$(4.6) \quad \begin{bmatrix} x^{(n+1)} - x^* \\ x^{(n)} - x^* \end{bmatrix} = \begin{bmatrix} (1+\gamma)I - \beta \tilde{A}_n & -\gamma I \\ I & 0 \end{bmatrix} \begin{bmatrix} x^{(n)} - x^* \\ x^{(n-1)} - x^* \end{bmatrix}.$$

We finally split \tilde{A}_n as $A_* + (\tilde{A}_n - A_*)$ in this equation to obtain (4.3).

We turn to estimate $\|p^{(n)}\|_2$ for $x^{(n)} \in U(x^*, \delta)$. As $\|p^{(n)}\|_2 \leq \beta \|A_* - \tilde{A}_n\|_2 \|x^{(n)} - x^*\|_2$, it suffices to bound $\|A_* - \tilde{A}_n\|_2$, which could be decomposed as

$$\|A_* - \tilde{A}_n\|_2 \leq \|A_* - B_n\|_2 + \|B_n - \tilde{A}_n\|_2, \quad B_n := \mathcal{P}_n \nabla^2 E(x^*).$$

By $\|\mathcal{P}_n\|_2 = 1$ and the ASSUMPTION 1, $\|B_n - \tilde{A}_n\|_2$ could be bounded as follows

$$(4.7) \quad \begin{aligned} \|B_n - \tilde{A}_n\|_2 &= \|\nabla^2 E(x^*) - \int_0^1 \nabla^2 E(x^* + t(x^{(n)} - x^*)) dt\|_2 \\ &\leq \int_0^1 \|\nabla^2 E(x^*) - \nabla^2 E(x^* + t(x^{(n)} - x^*))\|_2 dt \\ &\leq \int_0^1 t dt M \|x^{(n)} - x^*\|_2 = \frac{M}{2} \|x^{(n)} - x^*\|_2, \end{aligned}$$

where the second inequality is derived from the Lipschitz condition of the Hessian. On the other hand, $\|A_* - B_n\|_2$ is estimated by using Assumption 2

$$\begin{aligned}\|A_* - B_n\|_2 &\leq \|\nabla^2 E(x^*)\|_2 \|\mathcal{P}^* - \mathcal{P}_n\|_2 \\ &= 2\|\nabla^2 E(x^*)\|_2 \left\| \sum_{i=1}^k v_i^* v_i^{*\top} - \sum_{i=1}^k v_i^{(n)} v_i^{(n)\top} \right\|_2 \leq \frac{2\sqrt{2k}LM}{\mu} \|x^{(n)} - x^*\|_2.\end{aligned}$$

The last inequality follows from $\|\nabla^2 E(x^*)\|_2 \leq L$ and Corollary 4.1. Combining the above two equations we get (4.4) and thus complete the proof. \square

Based on the derived recurrence relation, we denote

$$F_{n+1} = \begin{bmatrix} x^{(n+1)} - x^* \\ x^{(n)} - x^* \end{bmatrix}, \quad T = \begin{bmatrix} (1+\gamma)I - \beta A_* & -\gamma I \\ I & 0 \end{bmatrix}, \quad P_n = \begin{bmatrix} p^{(n)} \\ 0 \end{bmatrix}$$

such that (4.3) could be simply represented as

$$(4.8) \quad F_{n+1} = TF_n + P_n.$$

THEOREM 4.6. *Suppose the Assumptions 1 and 2 hold. Given $\varepsilon \in (0, \frac{1}{\sqrt{\kappa}+1})$, $x^{(-1)} = x^{(0)}$, if $\|x^{(0)} - x^*\|_2 \leq \frac{\hat{r}}{2\sqrt{2}K}$, β and γ are chosen as (4.1), then $x^{(n)}$ converges to x^* with the estimate on the convergence rate*

$$(4.9) \quad \|x^{(n)} - x^*\|_2 \leq 2\sqrt{2}K\|x^{(0)} - x^*\|_2 \theta^n, \quad n \geq 0, \quad \theta := 1 - \frac{2}{\sqrt{\kappa}+1} + 2\varepsilon,$$

where $\hat{r} < \min\{\delta, \frac{\sqrt{3}\mu\varepsilon^2(\sqrt{\kappa}+1)^{3/2}}{16\sqrt{2}C_1}\}$, C_1 is given in (4.4) and K is defined in (4.2).

Proof. We derive from (4.8) that

$$(4.10) \quad F_{n+1} = T^{n+1}F_0 + \sum_{j=0}^n T^{n-j}P_j.$$

In order to employ Corollary 4.4 to bound T^m for $0 \leq m \leq n+1$ in (4.10), we need to show that A_* is a positive definite matrix. By the spectral decomposition $\nabla^2 E(x^*) = \sum_{i=1}^d \lambda_i^* v_i^* v_i^{*\top}$ we have

$$(4.11) \quad A_* = \left(I - 2 \sum_{i=1}^k v_i^* v_i^{*\top} \right) \sum_{j=1}^d \lambda_j^* v_j^* v_j^{*\top} = \sum_{i=1}^d h_i^* v_i^* v_i^{*\top},$$

where $h_i^* = -\lambda_i^*$ for $i = 1, \dots, k$ and $h_i^* = \lambda_i^*$ for $i = k+1, \dots, d$. Since x^* is an index- k saddle point, $h_i^* > 0$ for $1 \leq i \leq d$. By Assumption 1 and Corollary 4.4,

$$(4.12) \quad \|T^{n+1}F_0\|_2 \leq K(\sqrt{\gamma})^{n+1}\|F_0\|_2.$$

and

$$(4.13) \quad \left\| \sum_{j=0}^n T^{n-j}P_j \right\|_2 \leq \sum_{j=0}^n \|T^{n-j}P_j\|_2 \leq \sum_{j=0}^n K(\sqrt{\gamma})^{n-j}\|P_j\|_2 = \sum_{j=0}^n K(\sqrt{\gamma})^{n-j}\|p^{(j)}\|_2.$$

To get (4.9), it suffices to prove (A) $\|F_n\|_2 \leq 2K\theta^n\|F_0\|_2$ for all $n \geq 0$ with the support of the estimates (4.12)–(4.13). However, in order to bound $p^{(j)}$ in (4.13)

via (4.4), which is derived based on the properties in Assumption 1 that are valid only if $\|x^{(j)} - x^*\|_2 < \delta$, we also need to show that $(\mathbb{B}) \ \|F_n\|_2 \leq \hat{r} (< \delta)$ (such that $\|x^{(n)} - x^*\|_2 < \delta$) for all $n \geq 0$. Therefore, we intend to prove the two estimates (A) and (B) simultaneously by induction.

For $n = 0$, both (A) and (B) hold by the assumptions of this theorem and $K \geq C_0 \geq 1$ (cf. Corollary 4.4). Suppose both (A) and (B) hold for $0 \leq n \leq m$ for some $m \geq 1$, we obtain from (4.13) that

$$(4.14) \quad \begin{aligned} \left\| \sum_{j=0}^m T^{m-j} P_j \right\|_2 &\leq \sum_{j=0}^m K C_1 \beta (\sqrt{\gamma})^{m-j} \|F_j\|_2^2 \\ &\leq 2\beta K^2 C_1 \hat{r} \sum_{j=0}^m (\sqrt{\gamma})^{m-j} \theta^j \|F_0\|_2 \leq \frac{2\beta K C_1 \hat{r}}{\theta - \sqrt{\gamma}} \cdot K \theta^{m+1} \|F_0\|_2 \leq K \theta^{m+1} \|F_0\|_2, \end{aligned}$$

where in the first inequality we use results in Theorem 4.5, in the second inequality we bound $\|F_j\|_2^2$ by the induction hypotheses (A) and (B), in the third inequality we apply the estimate

$$\sum_{j=0}^n (\sqrt{\gamma})^{n-j} \theta^j = \theta^n \sum_{j=0}^n \left(\frac{\sqrt{\gamma}}{\theta} \right)^{n-j} \leq \frac{\theta^{n+1}}{\theta - \sqrt{\gamma}}$$

and in the last inequality we use the assumption $\hat{r} < \min\{\delta, \frac{\sqrt{3}\mu\varepsilon^2(\sqrt{\kappa}+1)^{3/2}}{16\sqrt{2}C_1}\}$ and the definitions of K , β , θ and γ to bound

$$\frac{2\beta K C_1}{\theta - \sqrt{\gamma}} \hat{r} = \frac{2C_1 \hat{r}}{\varepsilon} \left(\frac{2}{\sqrt{L} + \sqrt{\mu}} \right)^2 \frac{2\sqrt{2}(\sqrt{\kappa} + 1)^{1/2}}{\sqrt{3}\varepsilon} = \frac{16\sqrt{2}C_1}{\sqrt{3}\mu\varepsilon^2(\sqrt{\kappa} + 1)^{3/2}} \hat{r} < 1.$$

Combining (4.12), (4.14) and $\sqrt{\gamma} < \theta = \sqrt{\gamma} + \varepsilon$, we have $\|F_{m+1}\|_2 \leq 2K\theta^{m+1}\|F_0\|_2$ (i.e. the induction hypothesis (A) with $n = m + 1$), which, together with $\theta < 1$ and $\|F_0\|_2 = \sqrt{2}\|x^{(0)} - x^*\|_2 \leq \frac{\hat{r}}{2K}$, leads to

$$\|F_{m+1}\|_2 \leq 2K \cdot \frac{\hat{r}}{2K} = \hat{r}.$$

That is, (A) and (B) hold for $n = m + 1$ and thus for any $n \geq 0$ by induction, which completes the proof. \square

REMARK 2. If we choose $\varepsilon = \frac{1}{2(\sqrt{\kappa}+1)}$ in Theorem 4.6, the convergence rate $\theta = 1 - \frac{1}{\sqrt{\kappa}+1}$, which is faster than the $1 - \mathcal{O}(\frac{1}{\kappa})$ convergence rate of the standard discrete HiSD proved in [32], especially for large κ , i.e. ill-conditioned cases.

5. Numerical experiments. We present a series of numerical examples to demonstrate the efficiency of the A-HiSD algorithm in comparison with the HiSD (i.e. A-HiSD with $\gamma = 0$ in Algorithm 2.2). The same initial point will be used for both methods in each example.

5.1. Müller-Brown potential. We start with the well known Müller-Brown (MB) potential, a benchmark to test the performance of saddle point searching algorithms. The MB potential is given by [4]

$$E_{MB}(x, y) = \sum_{i=1}^4 A_i \exp[a_i(x - \bar{x}_i)^2 + b_i(x - \bar{x}_i)(y - \bar{y}_i) + c_i(y - \bar{y}_i)^2],$$

where $A = [-200, -100, -170, 15]$, $a = [-1, -1, -6.5, 0.7]$, $b = [0, 0, 11, 0.6]$, $c = [-10, -10, -6.5, 0.7]$, $\bar{x} = [1, 0, -0.5, -1]$ and $\bar{y} = [0, 0.5, 1.5, 1]$. We show the contour plot of MB potential in Fig.1a with two local minimas marked by red stars and the saddle point connecting them marked by a yellow solid point, as well as and trajectories of A-HiSD with different momentum parameters γ . The initial point is $(x^{(0)}, y^{(0)}) = (0.15, 1.5)$, the step size β is set as 2×10^{-4} and the SIRQIT is selected as the eigenvector solver.

As shown in Fig.1a, the trajectory of the HiSD method (i.e. the case $\gamma = 0$) converges to the saddle point along the descent path. A-HiSD utilizes the momentum term to accelerate the movement along the way such that less configurations appear on the trajectory as we increase γ . We also show the convergence behavior of four cases in Fig.1b, which indicates that a larger γ leads to the faster convergence rate. Since the problem is relatively well-conditioned, we do not need a very large γ to accelerate the convergence. This is consistent with our analysis.

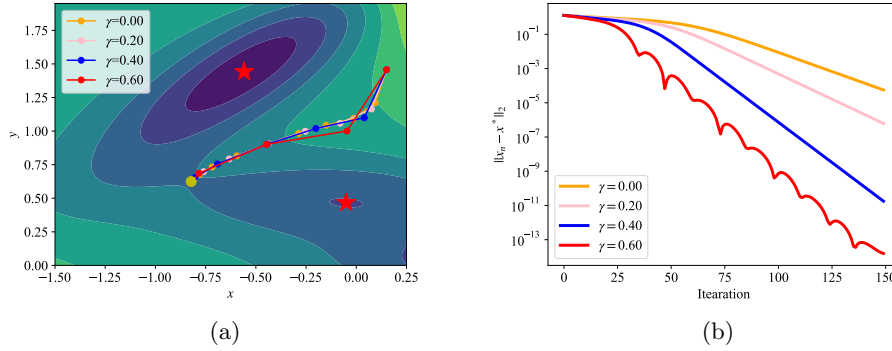


Fig. 1: (a) Contour plot of MB potential and trajectories of the A-HiSD with different γ . For a clear visualization, we plot configurations every 10 steps along the trajectory. (b) Plots of $\|x^{(n)} - x^*\|_2$ with respect to the iteration number.

Next we demonstrate the acceleration of the A-HiSD method by applying the modified MB potential [4]

$$E_{MMB}(x, y) = E_{MB}(x, y) + A_5 \sin(xy) \exp[a_5(x - \bar{x}_5)^2 + c_5(y - \bar{y}_5)^2].$$

The additional parameters are $A_5 = 500$, $a_5 = c_5 = -0.1$, $\bar{x}_5 = -0.5582$ and $\bar{y}_5 = 1.4417$. The landscape of modified MB potential is more winding compared with the MB potential. Similarly, we implement the A-HiSD method with different momentum parameters γ , the initial point $(x^{(0)}, y^{(0)}) = (0.053, 2.047)$ and the step size $\beta = 10^{-4}$. From Fig.2a we find that the HiSD method (i.e. the case $\gamma = 0$) follows the winding ascent path to approach the saddle point, which takes many gradient evaluations along the curved way, while A-HiSD method significantly relax the burden on gradient computations. By utilizing historical information, A-HiSD takes less iterations on the curved way to the saddle point. Furthermore, A-HiSD has the faster convergence rate as shown in Fig. 2b.

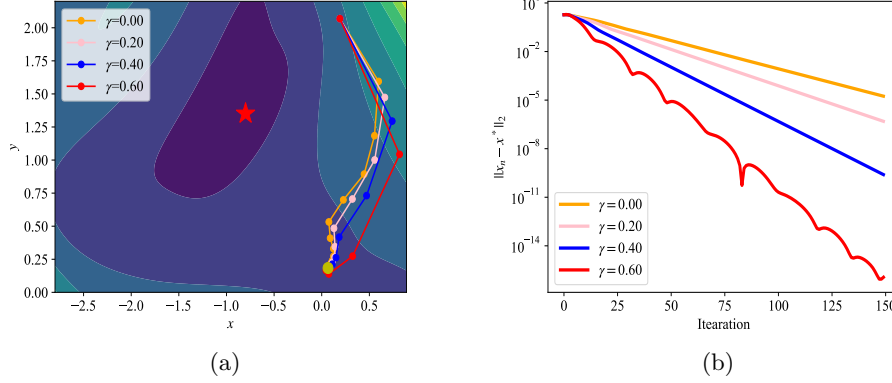


Fig. 2: (a) Contour plot of modified MB potential and trajectories of the A-HiSD with different γ . For a clear visualization, we plot configurations every 5 steps along the trajectory. (b) Plots of $\|x^{(n)} - x^*\|_2$ with respect to the iteration number.

5.2. Rosenbrock type function. The following experiments demonstrate the efficiency of A-HiSD method on high-dimensional ill-conditioned models. We consider the d -dimensional Rosenbrock function given by

$$R(x) = \sum_{i=1}^{d-1} [100(x_{i+1} - x_i^2)^2 + (1 - x_i)^2].$$

Here x_i is the i th coordinate of the vector $x = [x_1, \dots, x_d]^\top$. Note that $R(x)$ has a global minimum at $x^* = [1, \dots, 1]^\top$. We then modify $R(x)$ by adding extra quadratic arctangent terms such that x^* becomes a saddle point [32, 58]

$$(5.1) \quad R_m(x) = R(x) + \sum_{i=1}^d s_i \arctan^2(x_i - x_i^*).$$

We set $d = 1000$, $s_j = 1$ for $j > 5$ and (i) $s_i = -500$ or (ii) $s_i = -50000$ for $1 \leq i \leq 5$. We set $x^{(0)} = x^* + \rho \frac{n}{\|n\|_2}$ as the initial point where $n \sim \mathcal{N}(0, I_d)$ is a normal distribution vector and ρ is set as 1.0 for the case (i) and 0.1 for the case (ii).

We implement the A-HiSD under different γ to compare the numerical performance. Convergence behaviors of the case (i) are shown in Fig.3a. In this case, x^* is an index-3 saddle point and the condition number κ^* of $\nabla^2 R_m(x^*)$ is 721.93. The step size β is set as 5×10^{-4} and the eigenvector computation solver is set as the SIRQIT. Fig.3a indicates that the HiSD (i.e. $\gamma = 0$) has a slow converge rate, while increasing γ leads to a faster convergence rate. In particular, the A-HiSD with $\gamma = 0.95$ outperforms other situations, which achieves the machine precision within 1600 iterations. In comparison, the situation $\gamma = 0$ requires more than 2000 iterations to attain a low accuracy.

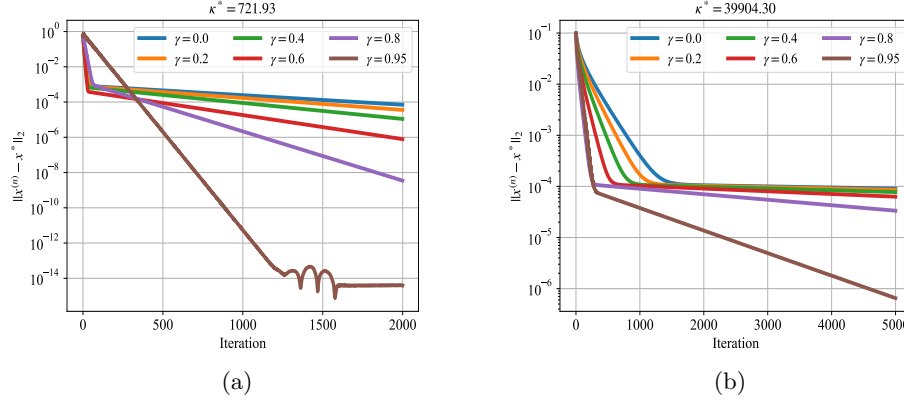


Fig. 3: Plots of $\|x^{(n)} - x^*\|_2$ with respect to the iteration number for the modified Rosenbrock function with (a) the condition (i) and (b) the condition (ii).

Results of the case (ii) are shown in Fig.3b. In this case, $\nabla^2 R_m(x^*)$ is more ill-conditioned compared with the case (i) since the condition number κ^* is 39904.29. Due to the ill-conditionedness, we have to choose a smaller step size $\beta = 2 \times 10^{-5}$ and select LOBPCG as the eigenvector solver. Meanwhile, x^* becomes an index-5 saddle point. All these settings make the case (ii) more challenging. We observe from Fig.3b that the convergence rate of the HiSD method is very slow as $x^{(n)}$ approaches the neighborhood of x^* , while the momentum term helps to release the problem by introducing the historical gradient information. For instance, A-HiSD with $\gamma = 0.95$ attains a remarkable faster convergence rate that outperforms other situations. Furthermore, as discussed in our numerical analysis, larger γ should be applied in ill-conditioned cases, which is consistent with the numerical observations.

5.3. Modified strictly convex 2 function. We compare the performance of A-HiSD method with another commonly-used acceleration strategy, i.e. the HiSD with the Barzilai-Borwein (BB) step size [3], which could accelerate the HiSD according to experiment results in [64, 58]. We apply the modified strictly convex 2 function, a typical optimization test example proposed in [41]

$$(5.2) \quad S(x) = \sum_{i=1}^d s_i a_i (e^{x_i} - x_i) / 10,$$

where $a_i = 1 + 5(i - 1)$ for $1 \leq i \leq d$, $s_i = -1$ for $1 \leq i \leq k$ and $s_j = 1$ for $k \leq i \leq d$. $x^* = [0, \dots, 0]$ is an index- k saddle point of $S(x)$. In our experiment, we set $d = 100$ and $k = 5$.

We implement A-HiSD method with different momentum parameters γ and compare with the HiSD with the BB step size β_n in each iteration

$$(5.3) \quad \beta_n = \min \left\{ \frac{\tau}{\|\nabla S(x^{(n)})\|_2}, \frac{\Delta x^{(n)\top} \Delta g^{(n)}}{\|\Delta g^{(n)}\|_2^2} \right\},$$

where $\Delta x^{(n)} = x^{(n)} - x^{(n-1)}$, $\Delta g^{(n)} = \nabla S(x^{(n)}) - \nabla S(x^{(n-1)})$ and $\tau = 0.5$ to avoid the too large step size. SIRQIT is selected as the eigenvector solver. The initial point $x^{(0)}$ is set as $[-6, \dots, -6]$.

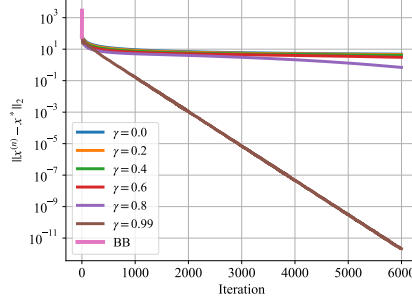


Fig. 4: Plots of $\|x^{(n)} - x^*\|_2$ with respect to the iteration number for the modified strictly convex 2 function. BB represents the HiSD method with the BB step size.

As shown in Fig.4, the HiSD with or without the BB step size diverges within a few iterations, while the A-HiSD method still converges. Meanwhile, as we increase γ , the convergence rate of the A-HiSD increases, which substantiates the effectiveness of the A-HiSD method in comparison with the HiSD with the BB step size.

5.4. Loss function of neural network. We implement an interesting, high-dimensional example of searching saddle points on the neural network loss landscape. Due to the non-convex nature of loss function, multiple local minima and saddle points are main concerns of the neural network optimization [13]. Recent research indicates that gradient-based optimization methods with small initializations can induce a phenomenon known as ‘saddle-to-saddle’ training process in various neural network architectures, including linear networks and diagonal linear networks [5, 24, 36]. In this process, network parameters may become temporarily stuck before rapidly transitioning to acquire new features. Additionally, empirical evidence suggests that vanilla stochastic gradient methods can converge to saddle points when dealing with class-imbalanced datasets—common occurrences in real-world datasets [40]. Consequently, it is urgent to figure out the impact of saddle points in deep learning. Analyzing saddle point via computations can provide valuable insights into specific scenarios.

Because of the overparameterization of neural networks, most critical points of the loss function are highly degenerate, which contains many zero eigenvalues. This challenges saddle searching algorithms since it usually leads to the slow convergence rate in practice.

Let $\{(x_i, y_i)\}_{i=1}^m$ with $x_i \in \mathbb{R}^{d_x}$ and $y_i \in \mathbb{R}^{d_y}$ be the training data. We consider a fully-connected linear neural network of depth H

$$(5.4) \quad f_{linear}(\mathbf{W}; x) = W_H W_{H-1} \cdots W_2 W_1 x,$$

where $\mathbf{W} = [W_1, W_2, \dots, W_H]$ with weight parameters $W_i \in \mathbb{R}^{d_{i+1} \times d_i}$ for $0 \leq i \leq H$ with $d_0 = d_x$ and $d_H = d_y$. The corresponding empirical loss L is defined by [1]

$$(5.5) \quad L(\mathbf{W}) = \sum_{i=1}^m \|f_{linear}(\mathbf{W}; x_i) - y_i\|_2^2 = \|W_H W_{H-1} \cdots W_2 W_1 X - Y\|_F^2.$$

where $X = [x_1, \dots, x_m]^\top$ and $Y = [y_1, \dots, y_m]^\top$. In practice we could vectorize W_1, \dots, W_H row by row such that L can be regarded as a function defined in \mathbb{R}^D

with $D = \sum_{i=1}^H d_i d_{i+1}$. According to [1], L contains a large amount of saddle points, which can be parameterized by the data set $\{(x_i, y_i)\}_{i=1}^m$. For instance, if $d_i = d_0$ for $1 \leq i \leq H-1$, then $\mathbf{W}^* := [W_1^*, \dots, W_H^*]$ is a saddle point where

$$(5.6) \quad W_1^* = \begin{bmatrix} U_{\mathcal{S}}^\top \Sigma_{YX} \Sigma_{XX}^{-1} \\ 0 \end{bmatrix}, \quad W_h^* = I \text{ for } 2 \leq h \leq H-1, \text{ and } W_H^* = [U_{\mathcal{S}} \quad 0].$$

Here I is the identity matrix, \mathcal{S} is an index subset of $\{1, 2, \dots, r_{\max}\}$ for $r_{\max} = \min\{d_0, \dots, d_H\}$, $\Sigma_{XX} = XX^\top$, $\Sigma_{YX} = YX^\top$, $\Sigma = \Sigma_{YX} \Sigma_{XX}^{-1} \Sigma_{YX}^\top$ and U satisfies $\Sigma = U\Lambda U^\top$ with $\Lambda = \text{diag}(\lambda_1, \dots, \lambda_{d_y})$. It is assumed in [1] that $\lambda_1 > \dots > \lambda_{d_y} > 0$, which holds true under the data of this experiment. $U_{\mathcal{S}}$ is then obtained by concatenating column vectors of U according to the index set \mathcal{S} .

In this experiments, we set the depth $H = 5$, the input dimension $d_x = 10$, the output dimension $d_y = 4$, $d_i = 10$ for $1 \leq i \leq 4$, and the number of data points $m = 100$. Data points (x_i, y_i) are drawn from the normal distributions $\mathcal{N}(0, I_{d_x})$ and $\mathcal{N}(0, I_{d_y})$, respectively. The initial point is $(W_1^{(0)}, \dots, W_H^{(0)}) = \mathbf{W}^* + (V_1, \dots, V_H)$ where (V_1, \dots, V_H) is a random perturbation whose elements $(V_h)_{i,j}$ are drawn from $\mathcal{N}(0, \sigma_h^2)$ independently, with $\sigma_h = 0.5 \frac{\|W_h^*\|_F}{\sqrt{d_{h-1} d_h}}$. Under the current setting, \mathbf{W}^* is a degenerate saddle point with 16 negative eigenvalues and several zero eigenvalues. Although A-HiSD is developed under the framework of non-degenerate saddle points, we show that this algorithm works well for the degenerate case. We set the step size $\beta = 0.1$ and the LOBPCG is selected as the eigenvector solver. Due to the highly degenerate property of the loss landscape, \mathbf{W}^* is not an isolated saddle point. Hence we compute the gradient norm instead of the Euclidean distance as the accuracy measure.

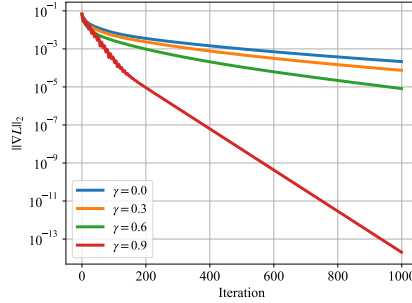


Fig. 5: Plots of the gradient norm $\|\nabla L\|_2$ with respect to the iteration number for the loss function of the neural network.

From Fig.5 we find that the A-HiSD with $\gamma = 0.9$ attains the tolerance 10^{-8} within 600 iterations, while that the HiSD (i.e. the case $\gamma = 0$) fails to converge. Furthermore, a faster convergence rate is achieved as we gradually increase γ , which indicates the great potential of A-HiSD method on the acceleration of convergence in highly degenerate problems.

6. Concluding remarks. We present the A-HiSD method, which integrates the heavy ball method with the HiSD method to accelerate the computation of saddle points. By employing the straightforward update formulation from the heavy

ball method, the A-HiSD method achieves significant accelerations on various ill-conditioned problems without much extra computational cost. We establish the theoretical basis for A-HiSD at both continuous and discrete levels. Specifically, we prove the linear stability theory for continuous A-HiSD and rigorously prove the faster local linear convergence rate of the discrete A-HiSD in comparison with the HiSD method. These theoretical findings provide strong supports for the convergence and acceleration capabilities of the proposed method.

While we consider the A-HiSD method for the finite-dimensional gradient system in this paper, it has the potential to be extended to investigate the non-gradient systems, which frequently appear in chemical and biological systems such as gene regulatory networks [38]. Furthermore, this method can be adopted to enhance the efficiency of saddle point search for infinite-dimensional systems, such as the Landau-de Gennes free energy in liquid crystals [21, 45]. Lastly, the effective combination of HiSD and the heavy ball method inspires the integration of other acceleration strategies with HiSD, such as the Nesterov accelerated gradient method [34] and the Anderson mixing [2]. We will investigate this interesting topic in the near future.

Acknowledgments. This work was supported by National Natural Science Foundation of China (No.12225102, T2321001, 12050002, 12288101 and 12301555), and the Taishan Scholars Program of Shandong Province.

REFERENCES

- [1] E. M. ACHOUR, F. MALGOUYRES, AND S. GERCHINOVITZ, *The loss landscape of deep linear neural networks: a second-order analysis*, 2022, <https://arxiv.org/abs/2107.13289>.
- [2] D. G. ANDERSON, *Iterative procedures for nonlinear integral equations*, J. ACM, 12 (1965), pp. 547–560.
- [3] J. BARZILAI AND J. M. BORWEIN, *Two-point step size gradient methods*, IMA J. Numer. Anal., 8 (1988), pp. 141–148.
- [4] S. BONFANTI AND W. KOB, *Methods to locate saddle points in complex landscapes*, J. Chem. Phys., 147 (2017), 204104.
- [5] E. BOURSIER, L. PILLAUD-VIVIEN, AND N. FLAMMARION, *Gradient flow dynamics of shallow relu networks for square loss and orthogonal inputs*, in Advances in Neural Information Processing Systems, vol. 35, Curran Associates, Inc., 2022, pp. 20105–20118.
- [6] R. E. BURTON, G. S. HUANG, M. A. DAUGHERTY, T. L. CALDERONE, AND T. G. OAS, *The energy landscape of a fast-folding protein mapped by Ala \rightarrow Gly substitutions*, Nat. Struct. Mol. Biol., 4 (1997), pp. 305–310.
- [7] Y. CAI AND L. CHENG, *Single-root networks for describing the potential energy surface of Lennard-Jones clusters*, J. Chem. Phys., 149 (2018), 084102.
- [8] E. CANCÈS, F. LEGOLL, M.-C. MARINICA, K. MINOUKADEH, AND F. WILLAIME, *Some improvements of the activation-relaxation technique method for finding transition pathways on potential energy surfaces*, J. Chem. Phys., 130 (2009), 114711.
- [9] C. J. CERJAN AND W. H. MILLER, *On finding transition states*, J. Chem. Phys., 75 (1981), pp. 2800–2806.
- [10] X. CHENG, L. LIN, W. E, P. ZHANG, AND A.-C. SHI, *Nucleation of ordered phases in block copolymers*, Phys. Rev. Lett., 104 (2010), 148301.
- [11] H. DANESHMAND, J. KOHLER, A. LUCCHI, AND T. HOFMANN, *Escaping saddles with stochastic gradients*, in Proceedings of the 35th International Conference on Machine Learning, J. Dy and A. Krause, eds., vol. 80 of Proceedings of Machine Learning Research, PMLR, 2018, pp. 1155–1164.
- [12] Y. N. DAUPHIN, R. PASCANU, C. GULCEHRE, K. CHO, S. GANGULI, AND Y. BENGIO, *Identifying and attacking the saddle point problem in high-dimensional non-convex optimization*, in Advances in Neural Information Processing Systems, vol. 27, Curran Associates, Inc., 2014.
- [13] Y. N. DAUPHIN, R. PASCANU, C. GULCEHRE, K. CHO, S. GANGULI, AND Y. BENGIO, *Identifying and attacking the saddle point problem in high-dimensional non-convex optimization*, NeurIPS, 27 (2014).
- [14] W. E, W. REN, AND E. VANDEN-EIJNDEN, *Simplified and improved string method for computing*

- the minimum energy paths in barrier-crossing events*, J. Chem. Phys., 126 (2007), 164103.
- [15] W. E AND X. ZHOU, *The gentlest ascent dynamics*, Nonlinearity, 24 (2011), 1831.
 - [16] K. FUKUMIZU, S. YAMAGUCHI, Y.-I. MOTOTAKE, AND M. TANAKA, *Semi-flat minima and saddle points by embedding neural networks to overparameterization*, in Advances in Neural Information Processing Systems, vol. 32, Curran Associates, Inc., 2019.
 - [17] W. GAO, J. LENG, AND X. ZHOU, *An iterative minimization formulation for saddle point search*, SIAM J. Numer. Anal., 53 (2015), pp. 1786–1805.
 - [18] N. GOULD, C. ORTNER, AND D. PACKWOOD, *A dimer-type saddle search algorithm with preconditioning and linesearch*, Math. Comp., 85 (2016), pp. 2939–2966.
 - [19] Y. HAN, Y. HU, P. ZHANG, AND L. ZHANG, *Transition pathways between defect patterns in confined nematic liquid crystals*, J. Comput. Phys., 396 (2019), pp. 1–11.
 - [20] Y. HAN, J. YIN, Y. HU, A. MAJUMDAR, AND L. ZHANG, *Solution landscapes of the simplified Ericksen–Leslie model and its comparison with the reduced Landau–de Gennes model*, Proc. R. Soc. A., 477 (2021), 20210458.
 - [21] Y. HAN, J. YIN, P. ZHANG, A. MAJUMDAR, AND L. ZHANG, *Solution landscape of a reduced Landau–de Gennes model on a hexagon*, Nonlinearity, 34 (2021), pp. 2048–2069.
 - [22] G. HENKELMAN AND H. JÓNSSON, *A dimer method for finding saddle points on high dimensional potential surfaces using only first derivatives*, J. Chem. Phys., 111 (1999), pp. 7010–7022.
 - [23] G. HENKELMAN AND H. JÓNSSON, *Improved tangent estimate in the nudged elastic band method for finding minimum energy paths and saddle points*, J. Chem. Phys., 113 (2000), pp. 9978–9985.
 - [24] A. JACOT, F. GED, B. ŞİMŞEK, C. HONGLER, AND F. GABRIEL, *Saddle-to-saddle dynamics in deep linear networks: Small initialization training, symmetry, and sparsity*, 2021, <https://arxiv.org/abs/2106.15933>.
 - [25] C. JIN, R. GE, P. NETRAPALLI, S. M. KAKADE, AND M. I. JORDAN, *How to escape saddle points efficiently*, in Proceedings of the 34th International Conference on Machine Learning, D. Precup and Y. W. Teh, eds., vol. 70 of Proceedings of Machine Learning Research, PMLR, 2017, pp. 1724–1732.
 - [26] C. JIN, P. NETRAPALLI, AND M. I. JORDAN, *Accelerated gradient descent escapes saddle points faster than gradient descent*, in Conference On Learning Theory, PMLR, 2018, pp. 1042–1085.
 - [27] D. P. KINGMA AND J. BA, *Adam: A method for stochastic optimization*, 2014, <https://arxiv.org/abs/1412.6980>.
 - [28] A. V. KNYAZEV, *Toward the preconditioned eigensolver: Locally optimal block preconditioned conjugate gradient method*, SIAM J. Sci. Comput., 23 (2001), pp. 517–541.
 - [29] Y. LI AND J. ZHOU, *A minimax method for finding multiple critical points and its applications to semilinear PDEs*, SIAM J. Sci. Comput., 23 (2001), pp. 840–865.
 - [30] D. E. LONGSINE AND S. F. MCCORMICK, *Simultaneous Rayleigh-quotient minimization methods for $Ax = \lambda Bx$* , Lin. Alg. Appl., 34 (1980), pp. 195–234.
 - [31] L. LUO, Y. XIONG, Y. LIU, AND X. SUN, *Adaptive gradient methods with dynamic bound of learning rate*, in Proceedings of the 7th International Conference on Learning Representations, New Orleans, Louisiana, 2019.
 - [32] Y. LUO, X. ZHENG, X. CHENG, AND L. ZHANG, *Convergence analysis of discrete high-index saddle dynamics*, SIAM J. Numer. Anal., 60 (2022), pp. 2731–2750.
 - [33] Y. NESTEROV, *Introductory Lectures on Convex Optimization: A Basic Course*, vol. 87, Springer Science & Business Media, 2003.
 - [34] Y. E. NESTEROV, *A method for solving the convex programming problem with convergence rate $O(1/k^2)$* , Sov. math. Dokl., 269 (1983), pp. 543–547.
 - [35] N. C. NGUYEN, P. FERNANDEZ, R. M. FREUND, AND J. PERAIRE, *Accelerated residual methods for the iterative solution of systems of equations*, SIAM J. Sci. Comput., 40 (2018), pp. A3157–A3179.
 - [36] S. PESME AND N. FLAMMARION, *Saddle-to-saddle dynamics in diagonal linear networks*, 2023, <https://arxiv.org/abs/2304.00488>.
 - [37] B. T. POLYAK, *Some methods of speeding up the convergence of iteration methods*, USSR Comput. Math. Math. Phys., 4 (1964), pp. 1–17.
 - [38] L. QIAO, W. ZHAO, C. TANG, Q. NIE, AND L. ZHANG, *Network topologies that can achieve dual function of adaptation and noise attenuation*, Cell Syst., 9 (2019), pp. 271–285.e7.
 - [39] W. QUAPP AND J. M. BOFILL, *Locating saddle points of any index on potential energy surfaces by the generalized gentlest ascent dynamics*, Theor. Chem. Acc., 133 (2014), p. 1510.
 - [40] H. RANGWANI, S. K. AITHAL, M. MISHRA, AND V. B. R., *Escaping saddle points for effective generalization on class-imbalanced data*, in Advances in Neural Information Processing Systems, vol. 35, Curran Associates, Inc., 2022, pp. 22791–22805.

- [41] M. RAYDAN, *The Barzilai and Borwein gradient method for the large scale unconstrained minimization problem*, SIAM J. Optim., 7 (1997), pp. 26–33.
- [42] S. J. REDDI, S. KALE, AND S. KUMAR, *On the convergence of Adam and beyond*, 2019, <https://arxiv.org/abs/1904.09237>.
- [43] A. SAMANTA, M. E. TUCKERMAN, T.-Q. YU, AND W. E, *Microscopic mechanisms of equilibrium melting of a solid*, Science, 346 (2014), pp. 729–732.
- [44] B. SHI, Y. HAN, J. YIN, A. MAJUMDAR, AND L. ZHANG, *Hierarchies of critical points of a Landau-de Gennes free energy on three-dimensional cuboids*, Nonlinearity, 36 (2023), p. 2631, <https://doi.org/10.1088/1361-6544/acc62d>.
- [45] B. SHI, Y. HAN, J. YIN, A. MAJUMDAR, AND L. ZHANG, *Hierarchies of critical points of a Landau-de Gennes free energy on three-dimensional cuboids*, Nonlinearity, 36 (2023), pp. 2631–2654.
- [46] G. W. STEWART AND J.-G. SUN, *Matrix perturbation theory*, Academic Press, San Diego, 1990.
- [47] D. WALES, *Energy Landscapes: Applications to Clusters, Biomolecules and Glasses*, Cambridge University Press, Cambridge, UK, 2003.
- [48] D. J. WALES AND J. P. DOYE, *Global optimization by basin-hopping and the lowest energy structures of Lennard-Jones clusters containing up to 110 atoms*, J. Phys. Chem. A, 101 (1997), pp. 5111–5116.
- [49] J.-K. WANG, C.-H. LIN, AND J. D. ABERNETHY, *A modular analysis of provable acceleration via Polyak’s momentum: Training a wide ReLU network and a deep linear network*, in International Conference on Machine Learning, PMLR, 2021, pp. 10816–10827.
- [50] W. WANG, L. ZHANG, AND P. ZHANG, *Modeling and computation of liquid crystals*, Acta Numer., 30 (2021), pp. 765–851.
- [51] Y. WANG AND J. LI, *Phase field modeling of defects and deformation*, Acta Mater., 58 (2010), pp. 1212–1235.
- [52] Z. XU, Y. HAN, J. YIN, B. YU, Y. NISHIURA, AND L. ZHANG, *Solution landscapes of the diblock copolymer-homopolymer model under two-dimensional confinement*, Phys. Rev. E, 104 (2021), p. 014505.
- [53] J. YIN, Z. HUANG, Y. CAI, Q. DU, AND L. ZHANG, *Revealing excited states of rotational bose-einstein condensates*, 2023, <https://arxiv.org/abs/2301.00425>.
- [54] J. YIN, Z. HUANG, AND L. ZHANG, *Constrained high-index saddle dynamics for the solution landscape with equality constraints*, J. Sci. Comput., 91 (2022), 62.
- [55] J. YIN, K. JIANG, A.-C. SHI, P. ZHANG, AND L. ZHANG, *Transition pathways connecting crystals and quasicrystals*, Proc. Natl. Acad. Sci. U.S.A., 118 (2021), e2106230118.
- [56] J. YIN, Y. WANG, J. Z. CHEN, P. ZHANG, AND L. ZHANG, *Construction of a pathway map on a complicated energy landscape*, Phys. Rev. Lett., 124 (2020), 090601.
- [57] J. YIN, B. YU, AND L. ZHANG, *Searching the solution landscape by generalized high-index saddle dynamics*, Sci. China Math., 64 (2021), pp. 1801–1816.
- [58] J. YIN, L. ZHANG, AND P. ZHANG, *High-index optimization-based shrinking dimer method for finding high-index saddle points*, SIAM J. Sci. Comput., 41 (2019), pp. A3576–A3595.
- [59] J. YIN, L. ZHANG, AND P. ZHANG, *Solution landscape of the Onsager model identifies non-axisymmetric critical points*, Phys. D: Nonlinear Phenom., 430 (2022), 133081.
- [60] Y. YU, T. WANG, AND R. J. SAMWORTH, *A useful variant of the Davis–Kahan theorem for statisticians*, Biometrika, 102 (2014), pp. 315–323, <https://doi.org/10.1093/biomet/asv008>.
- [61] J. ZHANG AND Q. DU, *Shrinking dimer dynamics and its applications to saddle point search*, SIAM J. Numer. Anal., 50 (2012), pp. 1899–1921.
- [62] L. ZHANG, *Construction of solution landscapes for complex systems*, Mathematica Numerica Sinica, 45 (2023), pp. 267–283.
- [63] L. ZHANG, L.-Q. CHEN, AND Q. DU, *Morphology of critical nuclei in solid-state phase transformations*, Phys. Rev. Lett., 98 (2007), 265703.
- [64] L. ZHANG, Q. DU, AND Z. ZHENG, *Optimization-based shrinking dimer method for finding transition states*, SIAM J. Sci. Comput., 38 (2016), pp. A528–A544.
- [65] L. ZHANG, P. ZHANG, AND X. ZHENG, *Error estimates for Euler discretization of high-index saddle dynamics*, SIAM J. Numer. Anal., 60 (2022), pp. 2925–2944.
- [66] L. ZHANG, P. ZHANG, AND X. ZHENG, *Discretization and index-robust error analysis for constrained high-index saddle dynamics on the high-dimensional sphere*, Sci. China Math., 66 (2023), pp. 2347–2360.
- [67] Y. ZHANG, Z. ZHANG, T. LUO, AND Z. J. XU, *Embedding principle of loss landscape of deep neural networks*, in Advances in Neural Information Processing Systems, vol. 34, Curran Associates, Inc., 2021, pp. 14848–14859.